


Article

Highly Precise Time Compensation Algorithm for Synchronous Communication System Based on Least Squares

Jin Su ¹, Changshui Li ¹, Qingbo Liu ¹, Sheng Zhao ¹ and Xiangyu Wang ^{2,*} ¹ Beijing Fibrlink Communications Co., Ltd., Beijing 100070, China² State Key Laboratory of Information Photonics and Optical Communications, Beijing University of Posts and Telecommunications, Beijing 100876, China

* Correspondence: xywang@bupt.edu.cn

Abstract: Time synchronization is an important technology in synchronous communication systems to ensure the accuracy of data transmission. Precise time synchronization allows the receiver to correctly interpret the signal at the correct moment. However, as communication rates increase and application scenarios diversify, pulse signal reception quality is often affected by factors such as noise interference and clock stability. In order to address these challenges, we propose a pulse signal recovery method utilizing the least squares algorithm to complete time compensation. By fitting and optimizing the received signal, we can obtain estimated values that closely approximate the actual time, thereby achieving enhanced precision in time synchronization. The results demonstrate that this method effectively reduces estimation errors, improving the system's time synchronization accuracy to the *ns* level. This method not only provides an effective solution for enhancing time synchronization precision but also lays the foundation for time synchronization performance in the future.

Keywords: time synchronization; synchronous communication system; time compensation; least squares algorithm



Academic Editor: Costantino De Angelis

Received: 21 November 2024

Revised: 31 December 2024

Accepted: 3 January 2025

Published: 9 January 2025

Citation: Su, J.; Li, C.; Liu, Q.; Zhao, S.; Wang, X. Highly Precise Time Compensation Algorithm for Synchronous Communication System Based on Least Squares. *Optics* **2025**, *6*, 2. <https://doi.org/10.3390/opt6010002>

Copyright: © 2025 by the authors. Licensee MDPI, Basel, Switzerland. This article is an open access article distributed under the terms and conditions of the Creative Commons Attribution (CC BY) license (<https://creativecommons.org/licenses/by/4.0/>).

1. Introduction

In applications such as Global Positioning Systems (GPSs), navigation systems [1–3], sensitive detection [4–6], and fundamental physics experiments [7–10], precise time synchronization between remote stations is critical. Traditional time synchronization methods have primarily relied on satellite systems [11–19], which have seen performance improvements with advancements in atomic clock technology in recent years. However, high-performance atomic clocks come with prohibitive costs, making them unsuitable for widespread deployment and portable applications. Additionally, the signal transmission paths in satellite-based systems are susceptible to various environmental factors, including multipath effects in the atmosphere, as well as delays and jitter introduced by the troposphere and ionosphere. In contrast, fiber-optic links offer significant advantages for time transfer [20–28], including low attenuation, wide bandwidth, and resistance to electromagnetic interference. These properties position fiber optics as a promising alternative medium for long-distance time transmission, providing high stability and reliability. Consequently, time synchronization over fiber-optic networks has garnered extensive research attention, leading to substantial advancements in the field. Researchers are actively exploring innovative techniques to leverage the unique characteristics of fiber optics, aiming to enhance synchronization accuracy and system robustness.

Accurate time synchronization over a wired channel is not only a prerequisite for ensuring that the two nodes send and receive data correctly. Despite the evolution of time synchronization technology, there are still many challenges in practical applications. First, malicious attacks, especially from eavesdroppers, can seriously affect the integrity of time synchronization by falsifying time signals or interfering with normal time transmission [29]. This type of attack can cause the recipient to be unable to obtain accurate data at a critical time, leading to a series of serious consequences. For example, in the financial trading system, the time deviation may lead to the wrong transaction order, which will cause economic losses. In power and energy management systems, inaccurate time synchronization may lead to scheduling errors and affect the stability and security of power supply. Second, the system's hardware inconsistencies and changes in environmental factors can also have a negative impact on time synchronization. These external interference sources not only introduce time deviation, but also increase the vulnerability of the system in a highly dynamic environment, especially in scenarios such as modern mobile synchronous communication; any small time error may lead to the wrong interpretation and processing of data, and even cause the overall failure of the system. In particular, in a high-speed synchronous communication system, the precision of the clock directly impacts the quality of data transmission [30–34]. Any slight clock jitter, even minute deviations, can lead to errors in the sampling time. Since data sampling is typically performed at fixed time intervals, if the clock experiences jitter, the sampling points will shift, causing discrepancies between the received data and the actual transmitted data. This sampling time error not only results in data deviations but may also lead to misjudgments or packet losses in subsequent processing stages, significantly affecting the overall performance and reliability of the system. In high-speed synchronous communication systems, where data transmission rates are extremely high, even small changes in clock precision can accumulate over multiple data cycles, causing errors to gradually amplify, ultimately affecting the stability of the entire communication link. Therefore, accurate clock synchronization and jitter control, especially in high-data-rate environments, are crucial for ensuring the efficient operation of the system and the accuracy of data transmission. Therefore, an effective time compensation method is necessary to improve the synchronization accuracy and stability of the realistic system.

In classical coherent optical communication, clock recovery algorithms have been extensively studied. Traditional clock recovery algorithms include the Mueller-Muller algorithm [35], the Godard algorithm [36], the early-late gate algorithm [37], and the Gardner algorithm [38]. Among these, the Mueller-Muller algorithm and the Godard algorithm have the advantage of requiring a relatively low ADC sampling rate, which requires only one sample per symbol rate. This reduces the hardware burden associated with high sampling rates. However, both algorithms are highly sensitive to the carrier phase and require additional carrier recovery steps in practical applications, which increases the complexity of digital signal processing at the receiver. The early-late gate algorithm, while less sensitive to the carrier phase, requires three samples per symbol period. This imposes higher demands on the ADC's sampling rate, significantly increasing hardware complexity in high-speed communications. The Gardner algorithm, on the other hand, only requires two samples per symbol rate, making it advantageous in terms of sampling rate requirements. However, it relies on processing multiple sampling points and calculating second derivatives, which adds computational complexity. As such, these algorithms all have certain limitations.

To address the limitations of traditional clock recovery methods in complex environments, we propose a clock compensation algorithm based on the least squares [39] method. This algorithm calibrates the received pulse signals directly and performs fitting to obtain more accurate sampling values, effectively compensating for time drift. It avoids the

high complexity of carrier recovery and the high sampling requirements inherent in traditional methods. Compared with conventional algorithms, the least squares-based method offers significant advantages: it simplifies the computation process, reduces hardware requirements, and maintains high computational efficiency even in scenarios involving large data volumes. Additionally, the least squares algorithm excels in flexibility, requiring no additional signal preprocessing steps, making it better suited to diverse application needs. By directly calibrating and optimizing the received pulse signals, our algorithm not only improves the accuracy of clock recovery but also significantly reduces computational complexity. Specifically, this paper simulates a time delay attack based on the actual synchronous communication process. Then, the data affected by time deviation is processed through the least squares algorithm. By comparing the difference between the actual received data and the fitted data, our method is able to identify and compensate for the time delay introduced by external interference. The results show that we can compensate and improve the time synchronization accuracy at the *ns* level. In contrast, the Gardner algorithm, a widely used clock recovery method, was also applied under the same conditions for comparison. Although Gardner can achieve time accuracy improvements in certain cases, its performance is generally inferior to that of the LS method. The results clearly indicate that the LS-based method outperforms Gardner in both accuracy and robustness, offering superior compensation for time deviations. This innovative approach not only significantly improves the accuracy of time synchronization but also enhances the system's overall reliability, ensuring the reliable reception of data across a wide range of application scenarios. These findings provide a new solution for advancing high-performance synchronous communication systems.

The rest of this paper is organized as follows. In Section 2, we introduce a practical optical communication system, the problem of time synchronization, and our proposed solution to this problem. In Section 3, we complete the simulation process based on the actual experiment, and compare the classical clock recovery algorithm and the compensation effect of least squares. Finally, we draw the conclusion in Section 4.

2. Problems and Method

In this section, we first describe the phenomenon of the frequency drift between the sender's and receiver's clocks. Then, we propose a method to solve the phenomenon.

2.1. Problems

Herein, the actual optical structure of the theoretical simulation is shown in Figure 1. At the sender's end, the laser is first injected into the modulator to complete the corresponding modulation, where the modulated electrical signal is generated by the arbitrary waveform generator (AWG). It is worth noting that due to the influence of the actual environment and other factors on the operating point of the modulator, the bias controller can be used to dynamically control the bias of the in-phase/quadrature (IQ) modulator, so as to obtain a stable output of the modulated signal.

After being transmitted over a classical channel of optical fiber, the signal is received by the receiver. In the receiver, the signal pulses interfere stably with the local oscillator that is produced by the same laser as the sender through the BS, after which both the outputs are followed by a variable optical attenuator for intensity match and fed into the balanced homodyne detector (BHD). After detection, the output signal of the BHD will be collected by the oscilloscope. In practice, the AWG and the oscilloscope were triggered by the same synchronous source to achieve clock synchronization at the transmitter and receiver.

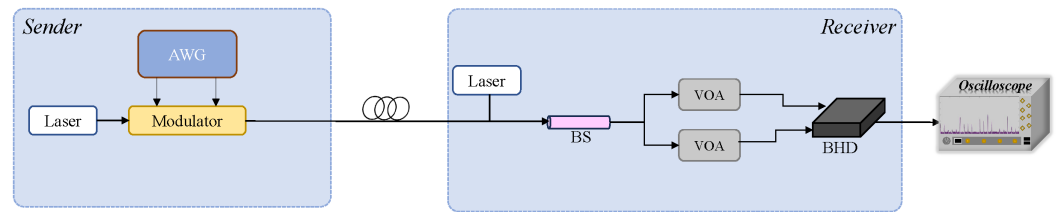


Figure 1. Actual optical structure of theoretical simulation. AWG: arbitrary waveform generator, BS: beam splitter, VOA: variable optical attenuator, BHD: balanced homodyne detector.

However, in practice, although the sender's and receiver's clocks have completed time synchronization, there may still be a relative drift in frequency. On the one hand, this relative drift comes from the frequency jitter of the two clocks, which is a hot topic in the field of digital communications. As we all know, crystal-controlled clock oscillators are the core of digital communication systems. The frequency instability of the crystal control clock is equivalent to adding an unintentional modulation to the signal due to noise generated by the active devices in the oscillator and buffer stage, crystal noise, and noise conducted by the power supply to the oscillator. On the other hand, external malicious attacks can also cause this phenomenon to occur. In particular, delay attacks from eavesdroppers can seriously affect the integrity of time synchronization by falsifying time signals or interfering with normal time transmission, resulting in the receiver being unable to obtain accurate data at critical moments. As shown in Figure 2, we can intuitively observe the time deviation caused by time jitter. Additionally, it is evident that once a time deviation occurs, the actual sampled data will also be affected, making it impossible to sample the data at the correct time.

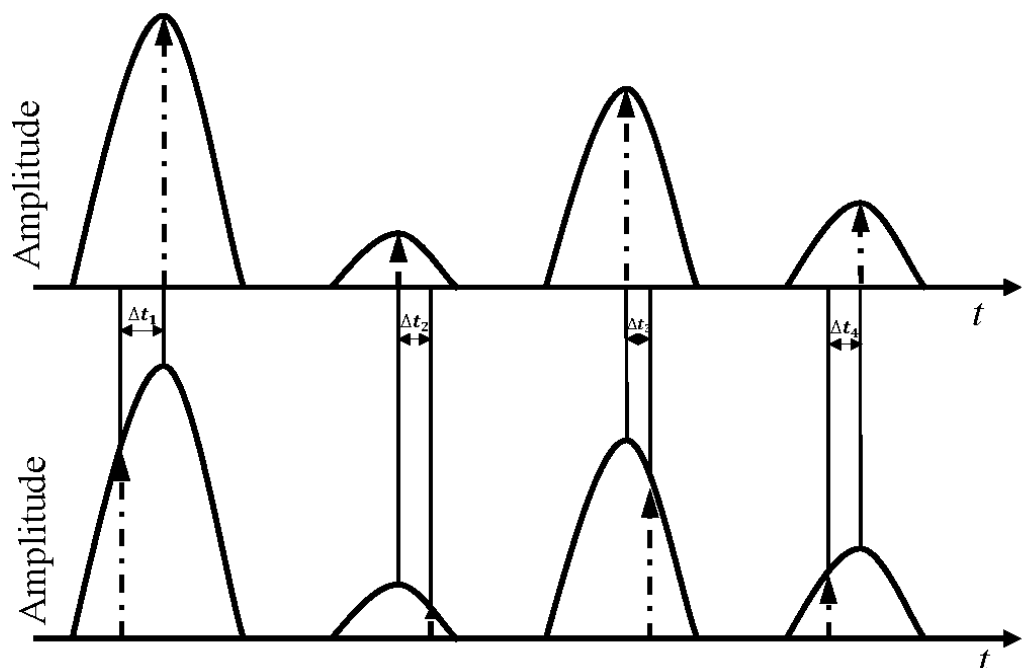


Figure 2. The description of sampling with clock drift in time varying between sender's and receiver's clocks (**lower**) and without clock drift (**upper**).

2.2. The Least Squares Algorithm

According to the above, in order to obtain the correct sampling value, make up for the time deviation caused by external factors, and improve the accuracy and robustness of the actual time synchronization, we propose a method to solve the phenomenon by the least squares (LS) algorithm. The LS algorithm is an optimization technique in statistics

and mathematics, widely used in data fitting and parameter estimation. It was initially proposed in the 19th century for the field of astronomy to address the problem of estimating unknown celestial orbits from measured data. The core idea is to find the optimal model parameters by minimizing the sum of squared errors between the observed data and the theoretical model. It is mainly used to fit curves or lines to estimate the trend or relationship of unknown data based on known data points. It is applicable to both linear and nonlinear models and ensures statistical significance and computational stability by minimizing the sum of squared residuals. The process of LS is shown in Figure 3.

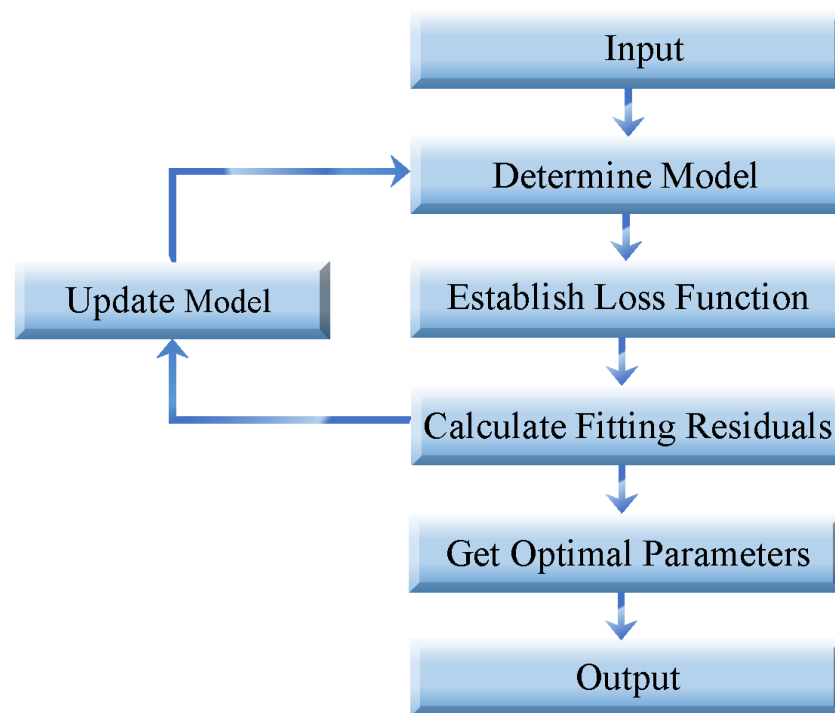


Figure 3. The process of least squares.

The first step is to acquire data. First, collect observational or experimental data for fitting to form a set of sample points, such as $(x_1, y_1), (x_2, y_2), \dots, (x_n, y_n)$, where x_i and y_i represents the observed value of the independent variable and the corresponding observed value of the dependent variable, respectively. Then, perform simple preprocessing on the collected data, such as removing or correcting outliers and eliminating noise, to ensure the quality of the acquired data. Preprocessing helps improve the final model fitting effect.

The second step is to determine the model. Specifically, the appropriate model is selected according to the characteristics of the data. LS generally includes a linear model and nonlinear model. A linear first-order model can generally be expressed as follows:

$$y = ax + b \quad (1)$$

Furthermore, taking the commonly used polynomial model as an example, a nonlinear model can generally be expressed as follows:

$$y = a_n x^n + a^{n-1} x_{n-1} + \dots + a_1 x + a_0 \quad (2)$$

It is worth noting that the order of the model is constantly optimized based on the data results.

The third step is to establish the loss function. In order to measure the effect of model fitting, the deviation between the observed data and the model prediction is usually defined as a loss function. It can be expressed by

$$L = \sum_{i=1}^n [(y_i - f(x_i; a_n, a_{n-1}, \dots, a_0))]^2 \quad (3)$$

where L represents the loss function, y_i represents the acquired data, and $f(x_i; a_n, a_{n-1}, \dots, a_0)$ represents the output of the model. Subsequently, the corresponding parameters are solved based on the loss function. In order to minimize the difference between the predicted value and the observed value, we need to take the partial derivative of each parameter and set it to zero. Therefore, the following equations can be expressed by

$$\left\{ \begin{array}{l} \frac{\partial L}{\partial a_n} = -2 \sum_{i=1}^n [f(x_i; a_n, a_{n-1}, \dots, a_0)] * x_i^n \\ \frac{\partial L}{\partial a_{n-1}} = -2 \sum_{i=1}^n [f(x_i; a_n, a_{n-1}, \dots, a_0)] * x_i^{n-1} \\ \dots \\ \frac{\partial L}{\partial a_1} = -2 \sum_{i=1}^n [f(x_i; a_n, a_{n-1}, \dots, a_0)] * x_i \\ \frac{\partial L}{\partial a_0} = -2 \sum_{i=1}^n [f(x_i; a_n, a_{n-1}, \dots, a_0)] \end{array} \right. \quad (4)$$

The fourth step is to calculate the fitting residuals, which represent the difference between the actual data and the fitted model, to evaluate the accuracy of the fitting. Here, the evaluation metric we use is the Mean Square Error (MSE).

Finally, the above process is repeated many times, and the optimal output is obtained by constantly updating the model.

3. Simulation and Results

According to the above experimental structure, we carried out the following simulation. First, a random pulse signal with a frequency of 5 MHz and a duty cycle of 20% is generated, and its waveform is shown in Figure 4a. To replicate the transmission process in a realistic manner, we incorporate several key factors that commonly affect fiber-optic communication channels. First, typical signal losses are introduced into the fiber channel. These losses are modeled using the actual fiber attenuation coefficient, where the power reduction over distance is represented mathematically by an exponential attenuation function. This accounts for the inherent loss in optical power as the signal propagates through the fiber. In addition to signal attenuation, we simulate time delays and phase jitter caused by environmental influences. Specifically, randomly distributed delays are introduced to emulate the impact of ambient temperature fluctuations, mechanical vibrations, and other external perturbations on the signal propagation speed. These delays are randomly drawn from a pre-defined distribution that captures the variability observed in real-world scenarios. Phase jitter, representing rapid, small deviations in the phase of the signal due to similar environmental factors, is also incorporated to simulate its adverse effects on synchronization and signal integrity. By introducing these impairments, the simulation environment closely resembles actual operating conditions. The combination of optical loss, random delays, and phase jitter creates a comprehensive scenario that allows us to evaluate the effectiveness of the proposed pulse signal recovery method under practical constraints. This detailed setup ensures that the simulation results provide meaningful insights into

the performance of the system in real-world deployments. Figure 4b shows the waveform of the ideal received signal with delay. At the receiving end, we use the sampling rate of 1 Gsa/s to sample the received signal, and the sampled waveform is shown in Figure 4c, from which can clearly see the attenuation and noise caused by channel transmission.

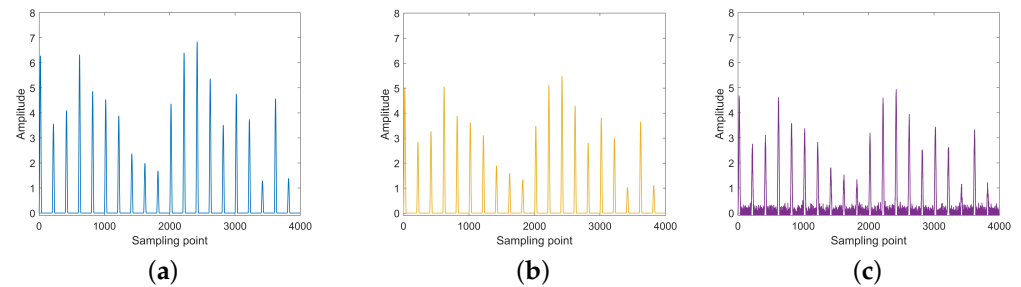


Figure 4. (a) The waveform of the initial signal. (b) The waveform of the ideal received signal with delay. (c) The waveform of the actual received signal with noise.

For the collected signals, we applied the LS process shown in Figure 3. By computing the fitted curve from the model and evaluating the fitting error against the predefined MSE threshold of 10^{-4} , we iteratively updated the model. Through this process, a fourth-order polynomial LS was selected, yielding the optimal parameters for the current model. The comparison of different waveforms after fitting is shown in the Figure 5. Among them, the blue solid line represents the initial signal sent, the orange solid line represents the ideal received signal, the yellow solid line indicates the signal received by external factors with delay, the purple solid line indicates the signal actually received with noise, and the final green solid line indicates the signal after LS processing. In order to make a more intuitive comparison, we have specially inserted an enlarged image of one of the pulses in the diagram. It can be seen that the waveform after LS is closer to the orange solid line than the actual received signal, which is the ideal received signal. It can be seen from this that LS has a good performance in terms of time compensation.

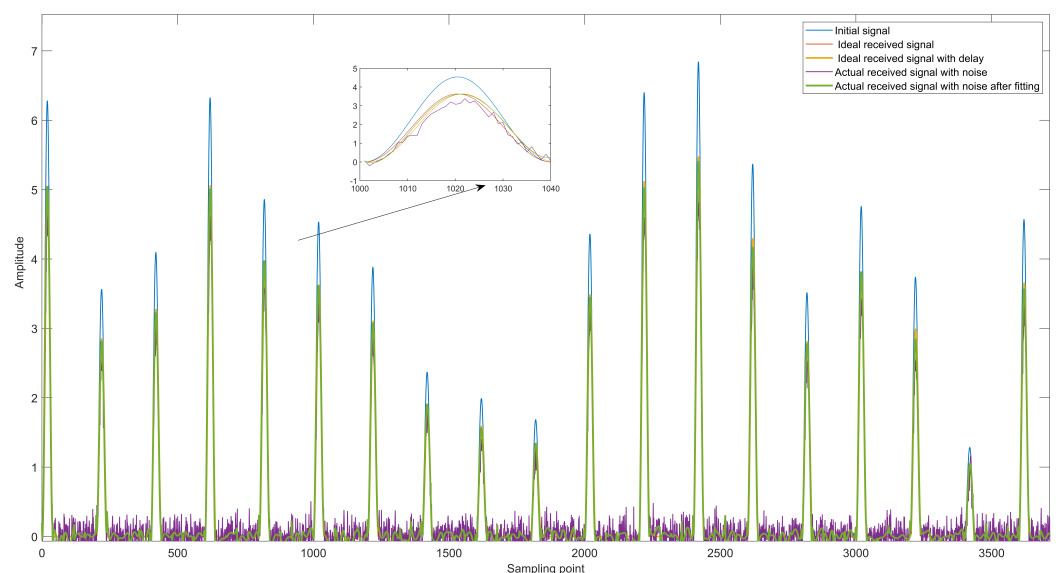


Figure 5. Comparison of different signal waveforms.

In addition to LS, the Gardner time recovery algorithm is also employed as a benchmark for comparison. Gardner's algorithm [38] is a widely adopted method in synchronous communication systems, particularly for its simplicity and efficiency. The core idea of Gardner's method lies in estimating the timing offset by identifying the zero-crossings of the

derivative of the received signal, with the goal of minimizing the timing error. This is achieved through a feedback loop that continuously adjusts the clock phase to align with the incoming signal. Despite its advantages in terms of computational simplicity, Gardner's algorithm is highly sensitive to noise and may struggle with complex distortions in the received signal.

To further analyze the effectiveness of LS processing, we compared it with the Gardner time recovery algorithm. The specific evaluation method is as follows: after the LS processing, we obtain the function expression of each pulse signal. At the same time, we find the maximum value of the actual received signal with noise in the same period. We record its sampling position and value as (x_1, y_{max}) . We put the value into the function and compute a new sampling position x_2 . Because our sampling rate is 1 Gsa/s, the time interval between each sampling point is $1ns$, so the corresponding improved time synchronization accuracy is $(x_2 - x_1)ns$. The improved accuracy of the whole received signal through LS is shown in Figure 6. Similarly, for the Gardner algorithm, before and after clock recovery, we also obtain different sampling values. The method for calculating the improved time precision for these different sampling values is the same as for LS. The improved accuracy of the whole received signal through the Gardner algorithm is also shown in Figure 6. It can be clearly seen that through LS processing, according to the calculation method proposed before, each pulse has improved the time accuracy at the ns level compared with the original. It can be clearly seen that, while both the LS and Gardner methods contribute to time recovery, LS demonstrates superior adaptability and robustness. According to the calculation method proposed before, LS has improved the time accuracy at the ns level compared with the original. Although Gardner can sometimes improve time precision to the nanosecond level, the overall precision enhancement is significantly lower than that achieved by LS. Moreover, in some cases, the improvement achieved by Gardner is even at the μs microsecond level.

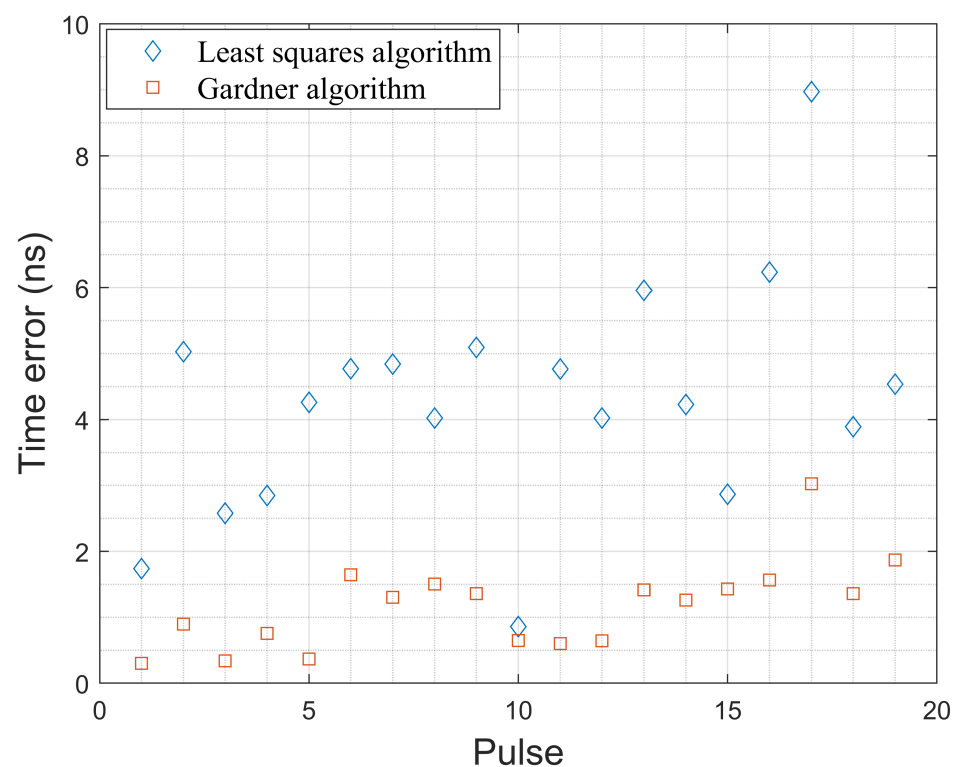


Figure 6. The description of the time accuracy that can be improved after the LS and Gardner algorithms.

4. Conclusions and Discussion

In this paper, we propose a new feasible method to complete time compensation to improve the accuracy and robustness of time synchronization. Based on the actual experiment process, we analyzed that in theory even under the guarantee of accurate time synchronization, once the deviation of the time synchronization system was caused by external factors, the final data would not be accurate. Therefore, we propose a novel time compensation method based on LS to address the above challenges. By fitting the received data, the method can estimate the ideal time value effectively, and then realizes the accurate prediction of synchronization state. Specifically, this paper simulates the whole process. By comparing the difference between the actual received data and the data after LS processing, the results show that we can compensate for this part of the deviation and improve the time synchronization accuracy at the *ns* level. In comparison, the Gardner algorithm, a traditional clock recovery method, was also tested under the same conditions. While Gardner showed improvements in time accuracy in some cases, its performance was generally less effective, with time compensation sometimes limited to the μs level. This difference highlights the superiority of the LS-based method in achieving higher precision and handling severe interference scenarios. Based on the improved time synchronization accuracy, it can directly support the higher running data rate in the synchronous communication system. Specifically, by compensating for nanosecond time deviations, the system can handle narrower pulses, which is essential to support higher frequency communications. In high-speed systems, even small time synchronization errors can lead to significant sampling errors, as is evident from our analysis. This method has the accuracy of nanoseconds and is convenient for the operation of a GHz synchronous communication system. However, the exact increase in data rate depends on several factors, such as modulation scheme, signal quality, channel conditions, and detection capabilities. These factors can be explored in future studies to quantify the precise impact on the operational data rate.

In conclusion, this innovative LS-based method not only significantly enhances the accuracy and robustness of time synchronization but also provides a feasible solution for ensuring reliable data reception in various application scenarios. By outperforming traditional methods like Gardner, the proposed approach offers a promising pathway for advancing high-performance synchronous communication systems and high-speed communication systems.

Author Contributions: Conceptualization, J.S., C.L., Q.L. and X.W.; methodology, J.S.; formal analysis, J.S. and C.L.; investigation, J.S.; resources, C.L. and S.Z.; writing—original draft preparation, J.S.; writing—review and editing, C.L., Q.L., S.Z. and X.W.; visualization, C.L.; supervision, C.L., Q.L., S.Z. and X.W.; project administration, C.L. and X.W. All authors have read and agreed to the published version of the manuscript.

Funding: This work was supported by the National Natural Science Foundation of China under Grant No. 62371060 and No. 62001041.

Institutional Review Board Statement: Not applicable.

Informed Consent Statement: Not applicable.

Data Availability Statement: Data underlying the results presented in this paper are not publicly available at this time but may be obtained from the authors upon reasonable request.

Conflicts of Interest: Author Jin Su, Changshui Li, Qingbo Liu, Sheng Zhao was employed by the company Beijing Fibrlink Communications Co., Ltd. The remaining authors declare that the research was conducted in the absence of any commercial or financial relationships that could be construed as a potential conflict of interest.

References

1. Li, X.; Ge, M.; Dai, X.; Ren, X.; Fritsche, M.; Wickert, J.; Schuh, H. Accuracy and reliability of multi-GNSS real-time precise positioning: GPS, GLONASS, BeiDou, and Galileo. *J. Geod.* **2015**, *89*, 607–635. [[CrossRef](#)]
2. Dow, J.M.; Neilan, R.E.; Rizos, C. The international GNSS service in a changing landscape of global navigation satellite systems. *J. Geod.* **2009**, *83*, 191–198. [[CrossRef](#)]
3. Lewandowski, W.; Arias, E. GNSS times and UTC. *Metrologia* **2011**, *48*, S219–S224. [[CrossRef](#)]
4. Marra, G.; Fairweather, D.; Kamalov, V.; Gaynor, P.; Cantono, M.; Mulholland, S.; Baptie, B.; Castellanos, J.; Vagenas, G.; Gaudron, J.O.; et al. Optical interferometry-based array of seafloor environmental sensors using a transoceanic submarine cable. *Science* **2022**, *376*, 874–879. [[CrossRef](#)] [[PubMed](#)]
5. Marra, G.; Clivati, C.; Luckett, R.; Tampellini, A.; Kronjäger, J.; Wright, L.; Mura, A.; Levi, F.; Robinson, S.; Xuereb, A.; et al. Ultrastable laser interferometry for earthquake detection with terrestrial and submarine cables. *Science* **2018**, *361*, 486–490. [[CrossRef](#)] [[PubMed](#)]
6. Clivati, C.; Tampellini, A.; Mura, A.; Levi, F.; Marra, G.; Galea, P.; Xuereb, A.; Calonico, D. Optical frequency transfer over submarine fiber links. *Optica* **2018**, *5*, 893–901. [[CrossRef](#)]
7. Boulder Atomic Clock Optical Network (BACON) Collaboration. Frequency ratio measurements at 18-digit accuracy using an optical clock network. *Nature* **2021**, *591*, 564–569. [[CrossRef](#)] [[PubMed](#)]
8. Delva, P.; Lodewyck, J.; Bilicki, S.; Bookjans, E.; Vallet, G.; Le Targat, R.; Pottie, P.E.; Guerlin, C.; Meynadier, F.; Le Poncin-Lafitte, C.; et al. Test of special relativity using a fiber network of optical clocks. *Phys. Rev. Lett.* **2017**, *118*, 221102. [[CrossRef](#)] [[PubMed](#)]
9. Lisdat, C.; Grosche, G.; Quintin, N.; Shi, C.; Raupach, S.; Grebing, C.; Nicolodi, D.; Stefani, F.; Al-Masoudi, A.; Dörscher, S.; et al. A clock network for geodesy and fundamental science. *Nat. Commun.* **2016**, *7*, 12443. [[CrossRef](#)]
10. Derevianko, A.; Pospelov, M. Hunting for topological dark matter with atomic clocks. *Nat. Phys.* **2014**, *10*, 933–936. [[CrossRef](#)]
11. Caldwell, E.D.; Sinclair, L.C.; Deschenes, J.D.; Giorgetta, F.; Newbury, N.R. Application of quantum-limited optical time transfer to space-based optical clock comparisons and coherent networks. *APL Photonics* **2024**, *9*, 016112. [[CrossRef](#)]
12. Shen, Q.; Guan, J.Y.; Ren, J.G.; Zeng, T.; Hou, L.; Li, M.; Cao, Y.; Han, J.J.; Lian, M.Z.; Chen, Y.W.; et al. Free-space dissemination of time and frequency with 10^{-19} instability over 113 km. *Nature* **2022**, *610*, 661–666. [[CrossRef](#)]
13. Schioppo, M.; Kronjaeger, J.; Silva, A.; Ilieva, R.; Paterson, J.; Baynham, C.; Bowden, W.; Hill, I.; Hobson, R.; Vianello, A.; et al. Comparing ultrastable lasers at 7×10^{-17} fractional frequency instability through a 2220 km optical fibre network. *Nat. Commun.* **2022**, *13*, 212. [[CrossRef](#)]
14. Gozzard, D.R.; Howard, L.A.; Dix-Matthews, B.P.; Karpathakis, S.; Gravestock, C.; Schediwy, S.W. Ultrastable free-space laser links for a global network of optical atomic clocks. *Phys. Rev. Lett.* **2022**, *128*, 020801. [[CrossRef](#)]
15. Shen, Q.; Guan, J.Y.; Zeng, T.; Lu, Q.M.; Huang, L.; Cao, Y.; Chen, J.P.; Tao, T.Q.; Wu, J.C.; Hou, L.; et al. Experimental simulation of time and frequency transfer via an optical satellite-ground link at 10^{-18} instability. *Optica* **2021**, *8*, 471–476. [[CrossRef](#)]
16. Khader, I.; Bergeron, H.; Sinclair, L.C.; Swann, W.C.; Newbury, N.R.; Deschênes, J.D. Time synchronization over a free-space optical communication channel. *Optica* **2018**, *5*, 1542–1548. [[CrossRef](#)]
17. Guo, Y.; Gao, S.; Bai, Y.; Pan, Z.; Liu, Y.; Lu, X.; Zhang, S. A new space-to-ground microwave-based two-way time synchronization method for next-generation space atomic clocks. *Remote Sens.* **2022**, *14*, 528. [[CrossRef](#)]
18. Kang, Y.; Wang, Q.; Wang, J.; Chen, R. A high-accuracy TOA-based localization method without time synchronization in a three-dimensional space. *IEEE Trans. Ind. Inform.* **2018**, *15*, 173–182. [[CrossRef](#)]
19. D’Amico, A.A.; Colavolpe, G.; Foggi, T.; Morelli, M. Timing synchronization and channel estimation in free-space optical OOK communication systems. *IEEE Trans. Commun.* **2022**, *70*, 1901–1912. [[CrossRef](#)]
20. Chen, X.; Lu, J.; Cui, Y.; Zhang, J.; Lu, X.; Tian, X.; Ci, C.; Liu, B.; Wu, H.; Tang, T.; et al. Simultaneously precise frequency transfer and time synchronization using feed-forward compensation technique via 120 km fiber link. *Sci. Rep.* **2015**, *5*, 18343. [[CrossRef](#)]
21. Zuo, F.; Xie, K.; Hu, L.; Chen, J.; Wu, G. 13 134-km fiber-optic time synchronization. *J. Light. Technol.* **2021**, *39*, 6373–6380. [[CrossRef](#)]
22. Chen, Y.; Dai, H.; Li, W.; Wang, F.; Wang, B.; Wang, L. Time reversal enabled fiber-optic time synchronization. *IEEE Trans. Instrum. Meas.* **2023**, *72*, 5503508. [[CrossRef](#)]
23. Dai, H.; Song, D.; Li, W.; Wang, G.; Pang, Z.; Li, C.; Wang, B. Hybrid fiber-based time synchronization and vibration detection system. *Opt. Lett.* **2024**, *49*, 3372–3375. [[CrossRef](#)] [[PubMed](#)]
24. Xu, X.; Zhang, Y.; Bian, Y.; Hu, J.; Dou, J.; Li, Y.; Xu, B.; Yu, S.; Guo, H. Controllable asymmetric attack against practical round-trip fiber time synchronization systems. *IEEE Photonics Technol. Lett.* **2023**, *35*, 1263–1266. [[CrossRef](#)]
25. Liu, Q.; Han, S.; Wang, J.; Feng, Z.; Chen, W.; Cheng, N.; Gui, Y.; Cai, H.; Han, S. Simultaneous frequency transfer and time synchronization over a 430 km fiber backbone network using a cascaded system. *Chin. Opt. Lett.* **2016**, *14*, 070602. [[CrossRef](#)]
26. Yu, Y.; Xu, J.; Liang, Y.; Li, F. Long Distance Optical Fiber Time Synchronization Technology and Accuracy Analysis. In Proceedings of the 2021 2nd International Conference on Artificial Intelligence and Education (ICAIE), Dali, China, 16–18 June 2021; pp. 141–149.

27. Chen, Z.; Yu, D.; Lu, G.; Zhang, Y.; Yu, S.; Luo, B.; Guo, H. Dual-comb-enhanced microwave clock synchronization over commercial fiber. *Optica* **2024**, *11*, 1268–1276. [[CrossRef](#)]
28. Lessing, M.; Margolis, H.; Brown, C.T.A.; Marra, G. Frequency comb-based time transfer over a 159 km long installed fiber network. *Appl. Phys. Lett.* **2017**, *110*, 221101. [[CrossRef](#)]
29. Manzo, M.; Roosta, T.; Sastry, S. Time synchronization attacks in sensor networks. In Proceedings of the 3rd ACM Workshop on Security of Ad Hoc and Sensor Networks, Alexandria, VA, USA, 7 November 2005; pp. 107–116.
30. Zhou, X. Efficient clock and carrier recovery algorithms for single-carrier coherent optical systems: A systematic review on challenges and recent progress. *IEEE Signal Process. Mag.* **2014**, *31*, 35–45. [[CrossRef](#)]
31. Stojanovic, N.; Gonzalez, N.; Xie, C.; Zhao, Y.; Mao, B.; Qi, J.; Binh, L. Timing recovery in Nyquist coherent optical systems. In Proceedings of the 2012 20th Telecommunications Forum (TELFOR), Belgrade, Serbia, 20–22 November 2012; pp. 895–898.
32. Li, Y.; Li, Y.; Dong, T.; Liu, Y.; Li, W.; Hong, X.; Qiu, J.; Yin, J.; Su, Y.; Wu, J. Real-time clock recovery algorithm with high clock frequency offset tolerance. *Opt. Commun.* **2021**, *493*, 127025. [[CrossRef](#)]
33. Tang, J.; Chen, H.; Cui, S.; Chen, Y.; Dai, L.; Zhou, K.; Liu, D. High receiver skew-tolerant and hardware-efficient clock recovery for short-reach coherent transmission. *Opt. Express* **2022**, *30*, 27064–27079. [[CrossRef](#)]
34. Sun, H.; Wu, K.T. Timing synchronization in coherent optical transmission systems. In *Enabling Technologies for High Spectral-Efficiency Coherent Optical Communication Networks*; John Wiley & Sons, Inc.: Hoboken, NJ, USA, 2016; pp. 355–394.
35. Musah, T.; Namachivayam, A. Robust timing error detection for multilevel baud-rate CDR. *IEEE Trans. Circuits Syst. I Regul. Pap.* **2022**, *69*, 3927–3939. [[CrossRef](#)]
36. Godard, D. Passband Timing Recovery in an All-Digital Modem Receiver. *IEEE Trans. Commun.* **1978**, *26*, 517–523. [[CrossRef](#)]
37. Guangyu, T.; Wenbing, C.; Hancheng, Z.; Yiwen, C.; Yang, T.; Xuehui, Y. Research and Implementation of the Early-late Gate Bit Synchronization Algorithm in the Non-coherent Spread Spectrum System. In Proceedings of the 2022 International Symposium on Networks, Computers and Communications (ISNCC), Shenzhen, China, 19–22 July 2022; pp. 1–4.
38. Gardner, F. A BPSK/QPSK timing-error detector for sampled receivers. *IEEE Trans. Commun.* **1986**, *34*, 423–429. [[CrossRef](#)]
39. Björck, Å. Least squares methods. *Handb. Numer. Anal.* **1990**, *1*, 465–652.

Disclaimer/Publisher’s Note: The statements, opinions and data contained in all publications are solely those of the individual author(s) and contributor(s) and not of MDPI and/or the editor(s). MDPI and/or the editor(s) disclaim responsibility for any injury to people or property resulting from any ideas, methods, instructions or products referred to in the content.